FULL PAPER

Single-Crystal-to-Single-Crystal Transformation of a Europium(III) Metal–Organic Framework Producing a Multi-responsive Luminescent Sensor

Xue-Zhi Song, Shu-Yan Song, Shu-Na Zhao, Zhao-Min Hao, Min Zhu, Xing Meng, Lan-Lan Wu, and Hong-Jie Zhang**

A sensor with a red-emission signal is successfully obtained by the solvothermal reaction of Eu^{3+} and heterofunctional ligand $bpydbH_2$ (4,4′-(4,4′-bipyridine-2,6-diyl) dibenzoic acid), followed by terminal-ligand exchange in a single-crystal-to-single-crystal transformation. As a result of treatments both before and after the metal–organic framework formation, accessible Lewis-base sites and coordinated water molecules are successfully anchored onto the host material, and they act as signal transmission media for the recognition of analytes at the molecular level. This is the first reported sensor based on a metal–organic framework (MOF) with multi-responsive optical sensing properties. It is capable of sensing small organic molecules and inorganic ions, and unprecedentedly it can discriminate among the homologues and isomers of aliphatic alcohols as well as detect highly explosive 2,4,6-trinitrophenol (TNP) in water or in the vapor phase. This work highlights the practical application of luminescent MOFs as sensors, and it paves the way toward other multi-responsive sensors by demonstrating the incorporation of various functional groups into a single framework.

1. Introduction

Governments and scientists have both been investing money and focussing attention towards environmental issues such as air, water, and industrial-waste pollution because they are detrimental to human health and sustainable development. Current commercial methods and technique-based instruments for pollution-detection are expensive and are not always available; thus, there is an urgent need for the development of novel methods that are highly efficient and can be easily applied to a broad range of pollutants.

Porous metal–organic frameworks (MOFs) are a flourishing subclass of porous crystalline materials, which comprise an assembly of metal cations or clusters and organic linkers; they have potential applications in gas-storage, separation methods, and catalysis.[1] Recently, MOFs have been investigated as chemical sensors capable of utilizing a range of host–guest interactions; many distinguished scientists have made pioneering contributions to this field.[2] In order to utilize host MOF materials for chemical detection, appropriate signal transduction must be incorporated; the sensitivity of the detection depends on it. The most common means of signal transduction is luminescence—a measurable quantity, which is often observable with the naked eye. Lanthanide-based MOFs (LnMOFs) have been used as fluorescent probes, thanks to the exceptional luminescent features of lanthanide ions, such as large Stokes shift values and pure, sharp emission lines arising from characteristic 4f electronic transitions.[3]

However, the synthesis of microporous LnMOFs is challenging due to the high coordination number and flexible coordination geometry of lanthanide ions.

Another, more pressing problem concerns how appropriate signal transmission media can be attached to luminescent MOFs; signal transmission requires specific recognition of analytes at the molecular level, and subsequently signal modulation with measurable change is needed. A variety of pre- and post-synthetic methods have been identified as high-performance routes for the functionalization of host MOFs. These routes may be advantageous for the introduction of a broad range of signal transmission media. Pre-synthetic methods involve the introduction of functional groups before the MOFs are formed.[4] Post-synthetic modification (PSM) refers to heterogeneous reactions of reactants with intact crystalline frameworks; such reactions include terminal-ligand removal, metal-ion exchange, and organic ligand decoration.[5] Previously, extensive studies on MOF-based sensors focused on one type of signal transmission medium: unsaturated metal centers or Lewis-base sites, which display excellent monofunctional sensing of single organic molecules, metal cations, or explosives.[6] The diversity of organic ligands and the availability of functionalized pore surfaces, however, should allow for multiple types of signal

Dr. X.-Z. Song, S.-Y. Song, S.-N. Zhao, Z.-M. Hao, M. Zhu, X. Meng, L.-L. Wu, Prof. H.-J. Zhang
State Key Laboratory of Rare Earth Resource Utilization
Changchun Institute of Applied Chemistry
Chinese Academy of Sciences
5625 Renmin Street, Changchun 130022, China
E-mail: songsy@ciac.ac.cn; hongjie@ciac.ac.cn
Dr. X.-Z. Song, S.-N. Zhao, Z.-M. Hao, M. Zhu, X. Meng, L.-L. Wu
University of Chinese Academy of Sciences
Beijing 100049, China

DOI: 10.1002/adfm.201303986

transmission media to be anchored, producing MOFs that can act as multi-responsive luminescent sensors.

In this work, the ligand 4,4′-(4,4′-bipyridine-2,6-diyl) dibenzoic acid ($bpydbH_2$)—which has been used by us and other groups[7] to construct porous (transition-metal)–organic frameworks—captures our attention again for the synthesis of porous LnMOFs. We were motivated to use this ligand again due to the following beneficial properties: i) its extreme rigidity, which is advantageous in the formation of porous structures; ii) its capacity to overcome the low absorption coefficient of single lanthanide ions through the antenna effect; and iii) its conjugated rings and available Lewis-base sites may enhance the sensing properties through various host–guest interactions. By reacting this ligand with europium, we successfully synthesized a highly stable europium-MOF-based sensor that exhibits a combination of uncoordinated Lewis-base sites and terminal aqua ligands; both pre- and post-synthetic methods are utilized, including a single-crystal-to-single-crystal transformation. This sensor exhibits multi-responsive luminescent sensing of small organic molecules, aliphatic alcohols, highly explosive 2,4,6-trinitrophenol (TNP), and inorganic ions in water.

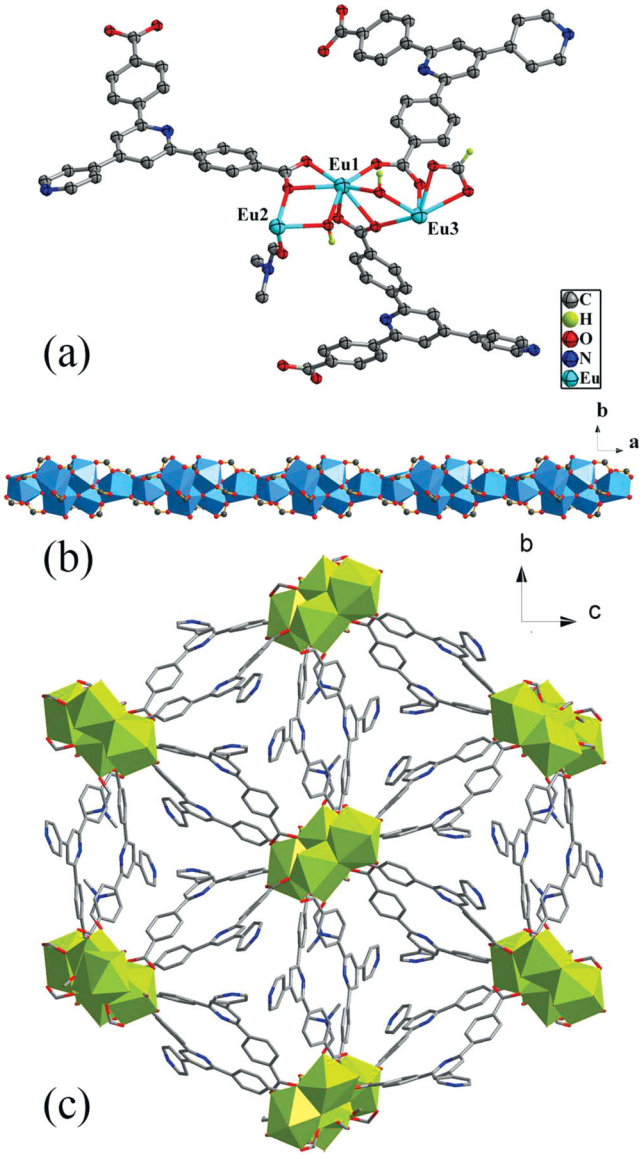

Figure 1. a) Ball-and-stick representation of the asymmetric unit in the crystal structure of **1**. Hydrogen atoms that are attached to the aromatic rings and lattice solvent molecules are omitted for clarity. b) Infinite 1D rod-like $[Eu_3(CO_2)_3(HCOO)(\mu_3\text{-}OH)_2]_n$, which acts as the SBU. c) Packing representation of **1** as viewed along the *a* axis. The blue and green polyhedra in (b) and (c) represent coordination spheres of Eu sites, while grey, blue, and red spheres/vertices represent C, N, and O centers, respectively.

2. Results and Discussion

2.1. Synthesis and Structure

The solvothermal reaction of the organic ligands $bpydbH_2$ and terephthalic acid (H_2BDC, benzene-1,4-dicarboxylic acid) with $Eu(NO_3)_3\cdot 6H_2O$ in a mixed solvent of *N,N*-dimethylformamide (DMF) and H_2O (6:1, v/v) afforded light yellow, rectangular-prismatic crystals of $[Eu_3(bpydb)_3(HCOO)(\mu_3\text{-}OH)_2(DMF)]\cdot(DMF)_3(H_2O)_2$ (**1**). Single-crystal X-ray diffraction revealed that compound **1** crystallizes in the space group $P2_1/n$. The asymmetric unit contains three crystallographically independent Eu^{3+} ions, three completely deprotonated $bpydb^{2-}$ anions, one formate anion, two μ_3-OH^- ligands, one terminally coordinated DMF ligand, three lattice DMF molecules, and two free water molecules (**Figure 1**a). The formate anion may be generated via the hydrolysis of DMF under solvothermal conditions.[8] The Eu1 ion is nona-coordinated by nine oxygen atoms: seven from four different $bpydb^{2-}$ ligands, and two from two μ_3-OH^- ligands, representing a tricapped triangular prismatic geometry. The Eu2 center is coordinated by eight oxygen atoms: four from four different $bpydb^{2-}$ ligands, three from μ_3-OH^- ligands, and one from the terminally coordinated DMF molecule. Meanwhile the Eu3 site is surrounded by eight oxygen atoms: three from two formate anions, one from an μ_3-OH^- ligand, and four from four different $bpydb^{2-}$ ligands. The local coordination geometries of the Eu2 and Eu3 ions are square antiprismatic and trigonal dodecahedron, respectively (Figure S1, Supporting Information (SI)). The Eu—O bond lengths range from 2.317(3) to 2.697(3) Å, which are comparable to those reported for other europium–oxygen donor complexes.[9] The carboxylate groups of the $bpydb^{2-}$ ligand are coordinated to metal centers and the 4,4′-bipyridine moieties are left free, owing to the greater affinity of rare-earth ions for oxygen donor atoms. The $bpydb^{2-}$ ligand acts as a μ_4-bridge, in which one carboxylate group adopts a μ_2-η^1:η^1-bridging mode, while the other adopts a μ_2-η^2:η^1-bridging mode (Figure S2, SI).

Adjacent Eu ions are bridged by carboxylate groups, with the aid of formate anions and μ_3-OH^- ligands, forming thick, infinite 1D chains along the *a* axis with Eu···Eu distances ranging from 3.659(3) to 4.159(3) Å (Figure 1b). These chains are further interconnected by $bpydb^{2-}$ ligands to construct a 3D non-interpenetrating framework. Utilization of these rod-like secondary building units (SBUs) has been shown to be an efficient strategy for the construction of robust porous lanthanide–organic frameworks.[10]

A single-crystal-to-single-crystal transformation (SC–SC) from **1** to another compound (**2**) occurs concomitant with the

replacement of the coordinated DMF ligands by an aqua ligand (vide infra). The framework of **2** is identical to **1**; 1D channels along the *b* axis accommodate the newly coordinated aqua ligand and the disordered solvent molecules. PLATON analysis revealed that the 3D porous structure contains large voids of 2448.8 Å^3, which represents 29.7% of the volume of the unit cell when the disordered solvent molecules are removed.[11]

2.2. Single-Crystal-to-Single-Crystal Transformation, Gas Adsorption, and Stability

X-ray single-crystal analysis (Figure S3, SI) indicated that the coordinated DMF ligand and the lattice solvent DMF molecules in **1** are replaced by an aqua ligand and other disordered solvent molecules, respectively, generating the new single-crystalline material $[Eu_3(bpydb)_3(HCOO)(\mu_3\text{-}OH)_2(H_2O)]\cdot(x$ solvent) (**2**) via a SC–SC transformation. The observed power X-ray diffraction (PXRD) patterns for the as-synthesized bulk samples of **1** and **2** are in good agreement with those simulated on the basis of the single-crystal X-ray diffraction data, confirming the phase purity of the as-synthesized products (**Figure 2**a). In the IR spectra, the strong vibration at 1666 cm^{-1}—corresponding to coordinated DMF—is absent in **2**, indicating a complete SC–SC transformation.[7d,12]

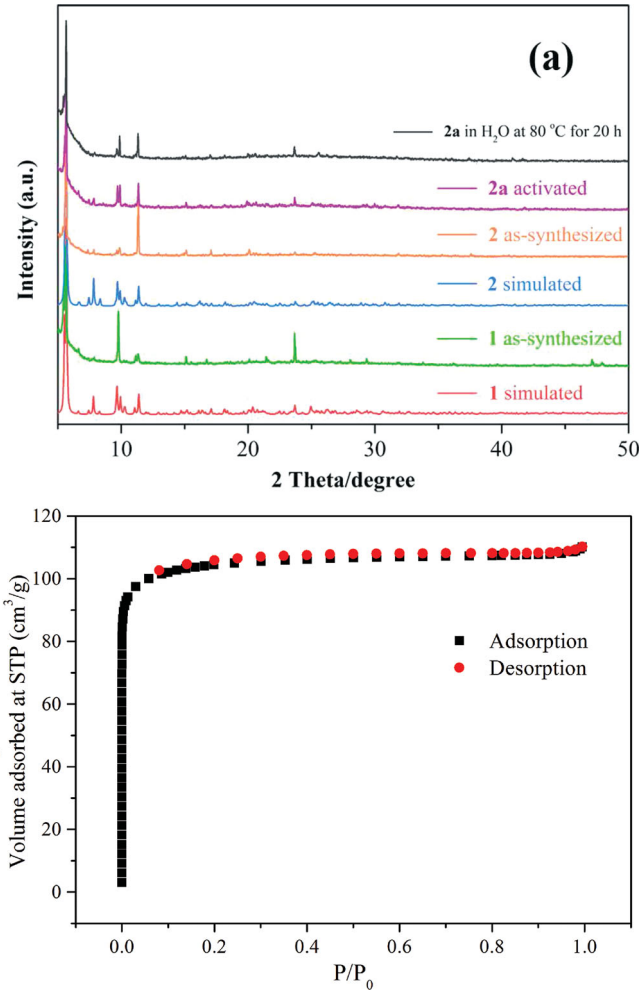

Figure 2. a) PXRD patterns of **1** and **2**. b) N_2-adsorption isotherm of activated **2a** at 77 K; STP and P/P_0 represent standard temperature and pressure and relative pressure, respectively.

Thermal activation of **2** at 150 °C under vacuum for 15 h gave rise to activated **2a**, in which the aqua ligand was retained, as confirmed by elemental analysis and Fourier-transform (FT) IR spectra (Figure S4, SI). The permanent microporous structure of the activated **2a** was further established by its N_2 sorption isotherm at 77 K, which displays typical type-I sorption behavior, with a Brunauer–Emmett–Teller (BET) surface area of 316.20 m^2 g^{-1} (Figure 2b and Figure S6, SI). Water stability is a pertinent issue for any host material that has the potential to be used in so many important applications, especially for industry.[13] The water stability of activated **2a** was examined by soaking activated samples in water at 80 °C for 20 h. PXRD patterns of the treated samples strongly indicate that the crystalline integrity of the porous framework is retained, especially under hydrothermal conditions (Figure 2a). The high hydrothermal stability of **2a** can be attributed to the combination of the rod-like SBUs and the strong coordination interactions between Eu^{3+} and the carboxylate groups.[14] The porous structure, aromatic rings directed into the channels, accessible Lewis-base sites, and the high hydrothermal stability of the material were sufficiently appealing to warrant testing the sensing properties of activated **2a** as a host material.

2.3. Photoluminescent Properties and Sensing of Organic Solvent Molecules

The excitation and photoluminescent (PL) spectra of activated **2a** are shown in the SI (Figure S7). The excitation spectrum of **2a**, monitored under the characteristic emission (615 nm) of the Eu^{3+} ion, exhibits a broad band with a maximum at 362 nm and a shoulder peak at 320 nm, and one sharp line at 467 nm. The broad excitation band is assigned to the absorption of the organic ligands, while the sharp line at 467 nm—much weaker compared to the excitation band of the organic ligands—may be ascribed to the $^7F_0 \rightarrow {}^5D_2$ transition of the Eu^{3+} ion. Upon excitation at 362 nm, the emission spectra of **2a** reveals well-resolved peaks centered at 593, 615, 650, and 699 nm, corresponding to the f–f electronic transitions ($^5D_0 \rightarrow {}^7F_J$, J = 1–4) of the Eu^{3+} ion, with the hypersensitive $^5D_0 \rightarrow {}^7F_2$ transition dominating the spectra. The broad emission band centered at 450 nm, originating from the organic ligands, is observed, but it is much weaker than the metal-based red emission. This demonstrates that the organic ligand is capable of sensitizing the luminescence of the Eu(III) ion; however, it is not completely effective.

The characteristic bright-red luminescence of **2a** primarily drove us to investigate its potential for sensing common organic solvent molecules. Finely ground samples of pre-activated **2a** of known amount were immersed in different organic solvents (methanol, ethanol, acetone, 1,4-dioxane, acetonitrile, chloroform, dichloromethane, ethyl acetate, tetrahydrofuran, and DMF), treated with ultrasonication, and then aged to form stable emulsions prior to fluorescence measurements. As shown in **Figure 3**, the intensities of **2a** in the PL spectra excited at 320 nm are strongly dependent on the solvent, particularly for acetone,

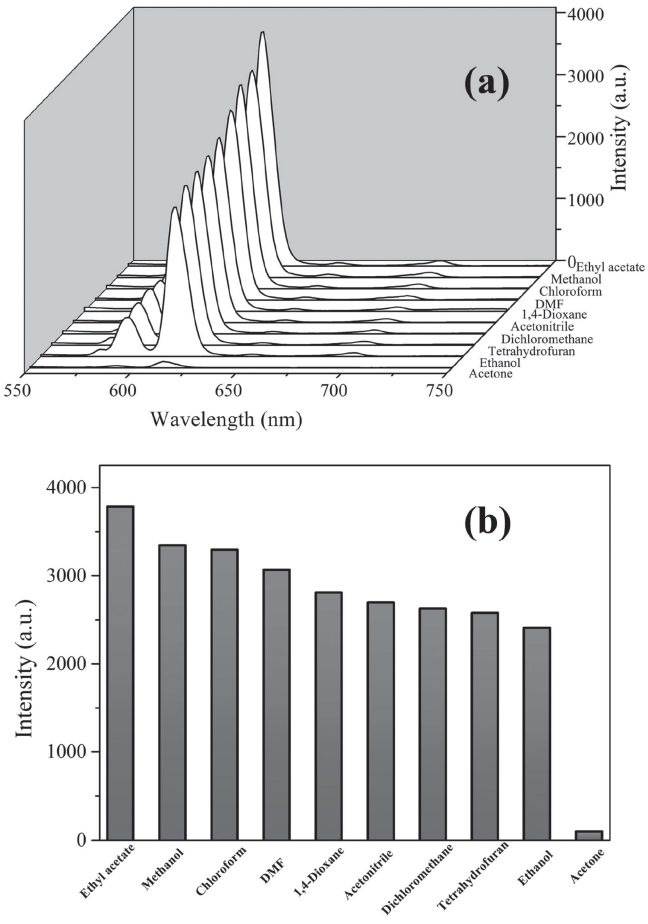

Figure 3. a) PL spectra and b) the $^5D_0 \rightarrow {}^7F_2$ transition intensities of the **2a** samples that were introduced into various pure solvents. Excitation: 320 nm.

which exhibits the most significant quenching effect. Such solvent-dependent luminescent properties are of significant interest in the sensing of acetone, which is very harmful to human health. The mechanism of the quenching effect was investigated by UV–vis absorption spectroscopy (Figure S8, SI). Among the solvents studied, acetone has an observable absorption intensity at 320 nm, while no other solvents absorbs at this wavelength. Upon illumination, there is competition between the absorption of acetone and the excitation of **2a**, resulting in a decrease (even quenching) in PL intensity. However, no similar quenching was observed under excitation at 362 nm, which indicates the validity of this quenching mechanism because acetone does not absorb at 362 nm (Figure S9, SI). The quenching mechanism is consistent with one previously proposed by Chen and co-workers and by us,[15] but it is different from the binding-interaction mechanism between the luminescent open-metal sites and guest solvent molecules that is also described in the literature.[16]

2.4. Discriminating the Homologues and Isomers of Aliphatic Alcohols

In addition to its sensing capabilities of common solvent molecules, the sensing response of **2a** for aliphatic alcohols was also investigated. The fluorescence signals of **2a**-containing suspensions in different pure aliphatic alcohols ($CH_3(CH_2)_nOH$, where n = 0, 1–5, and $(CH_3)_2CHOH$) were measured. The PL intensities decreased with increasing length of the linear carbon chains in the primary alcohols. More notably, the PL intensity of the suspension in *n*-propanol was more than two times stronger than that measured for the suspension in isopropanol (*i*-propanol) (**Figure 4**a). For a more detailed investigation, equivalent aliquots of **2a** were dispersed in *n*- and *i*-propanol mixtures of various proportions to monitor the emissive response. The luminescent intensity gradually decreased as the volume content of *i*-propanol increased (Figure 4b). The decreasing trend of the luminescent intensity of the $^5D_0 \rightarrow {}^7F_2$ transition of Eu^{3+} at 615 nm versus the volume content of *i*-propanol fits well with a first-order exponential function (R^2 = 0.99911). Interestingly, in the literature, sensor-based luminescent intensities in these two isomers of propanol are approximately equal.[16,17] Thus, the regular luminescent change of **2a**-containing suspensions in different alcohols indicates that the host material possesses the ability to recognize and sense the homologues and isomers of aliphatic alcohols. To the best of our knowledge, this is the first MOF-based sensor with this specific property.

Although the mechanism for the recognition and sensing effect is not clear at this moment, the host–guest interaction between **2a** and the guest aliphatic alcohol definitely plays an important role. The accessible nitrogen atoms of the pyridyl rings and the aqua ligands in **2a** may interact with the guest alcohol molecules through hydrogen bonds. Increasing the chain length of the primary aliphatic alcohols results in fewer such interactions due to lipophilic chains blocking the active sites (Figure S10, SI). The ability to differentiate between propanol isomers may originate from the differences in steric hindrance.

2.5. Sensing of Highly Explosive TNP

Aromatic compounds are one major form of industrial raw materials and are ubiquitous in plastic processing, refinery operations, and fuel operations; they are potentially carcinogenic and neurotoxic. The characteristic, bright-red luminescence and extensively aromatic structure of the host material **2a** provides the possibility of sensing target aromatic molecules via specific host–guest interactions. Identical volumes (25 μL) of different aromatic compounds were added to a standard emulsion of **2a** in DMF in order to detect the emissive response. A nearly complete luminescence quenching effect was only observed for nitrobenzene (NB). It was further found that the fluorescent intensity of the emulsion of **2a** decreased with increasing amounts of NB; the decreasing trend of the intensity at 615 nm versus the molar concentration fits well to a first-order exponential decay (Figure S11, SI). As a result, the selective luminescence quenching by NB is likely due to the electron transfer from the aromatic rings of the $bpydb^{2-}$ ligand to the electron-deficient NB.

The primary result of the sensing tests with electron-deficient NB inspired us to investigate the possibility of sensing other nitro-compounds, some of which are associated with highly explosive materials. Fluorescence quenching titrations

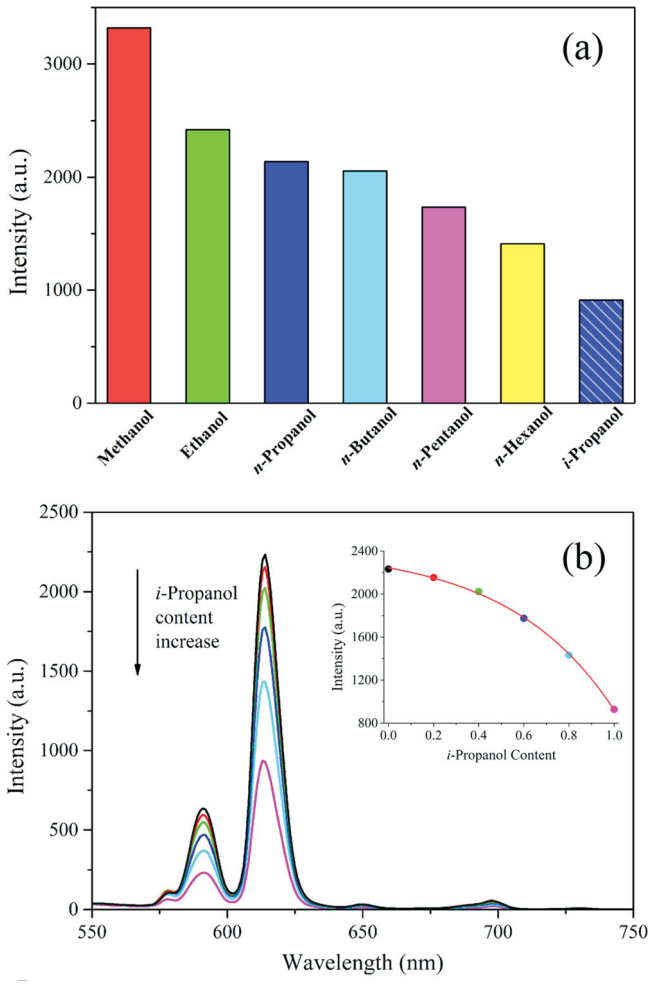

Figure 4. a) The $^5D_0 \rightarrow {}^7F_2$ transition intensities of **2a** that was introduced into various pure aliphatic alcohols (excitation wavelength, $\lambda_{ex} = 362$ nm). b) PL spectra of **2a** that was introduced into *n*- and *i*-propanol mixtures with increasing *i*-propanol volume content from 0 to 1 (top-to-bottom). Inset: The PL intensity as a function of *i*-propanol volume content.

were performed with the nitro-compounds, 2,4,6-trinitrophenol (TNP), 4-nitrophenol (4-NP), 3-nitrophenol (3-NP), *ortho*-nitrotoluene (*o*-NT), *meta*-nitrotoluene (*m*-NT), nitrobenzene (NB), and nitromethane (NM). All seven nitro-compounds can weaken the photoluminescent intensity of the **2a** emulsion to different degrees. The order of quenching efficiency is TNP > 4-NP > 3-NP >*o*-NT >*m*-NT > NB > NM, with the largest quenching percentage (QP) of 75% for TNP in DMF solution. The higher quenching efficiency for TNP compared to the other nitro-compounds indicated a high selectivity for TNP (Figure S12, SI).

The hydrothermal stability of **2a** may make it useful as a TNP-sensor in aqueous systems. The same fluorescence quenching titration experiment was performed using H_2O in place of DMF. The fluorescent intensity decreased continuously upon incremental addition of an aqueous TNP solution (1 mM) into a standard **2a** emulsion in H_2O. The fluorescence quenching by TNP could be detected at low concentration (4.98 μM; **Figure 5**a). The Stern–Volmer plots of relative luminescent intensity (I_0/I) versus the TNP concentration are shown in Figure 5b to further quantify the quenching efficiency, where I_0 and I are the fluorescence intensity of the emulsion in the absence and presence of the analyte, respectively. It is notable that the I_0/I versus TNP concentration plots bend upwards instead of being the typically linear plots; this may be attributed to the presence of simultaneous static and dynamic quenching.[18] Nonlinear Stern–Volmer curves in aqueous and DMF systems can be well-fit to the exponential equations of $I_0/I = 2.37e^{8879.3[TNP]} - 1.45$ and $I_0/I = 1.98e^{7700.9[TNP]} - 1.01$ with quenching constants of 2.1×10^4 and $1.5 \times 10^4 M^{-1}$, respectively, in the low-concentration range. The quenching constant of **2a** for TNP in the aqueous system is higher than those found for supramolecular-polymer-based sensors,[19] and it is comparable to those of known organic polymers and one recent example of a MOF-based sensor.[20] It is lower, however, than the value measured for AIE luminogen-functionalized sensors (AIE: aggregation-induced emission).[21]

To better understand the high quenching efficiency of **2a** towards TNP, especially in aqueous solution, the quenching mechanism was investigated in detail. Generally, the mechanism of quenching effects of MOFs for nitro-compounds have been well documented: upon excitation, electrons are typically transferred from the conduction band (CB) to the lowest unoccupied molecular orbitals (LUMOs) of analytes because the CB energy level of MOFs is higher than the LUMOs of analytes.[22] The different bandgaps between the CB of the MOF and the LUMOs of the analytes may confer various driving forces for electron transfer. Additionally, stronger excited light absorption by the analytes results in greater quenching efficiency, as was observed for acetone. As exhibited in the UV–vis absorption spectra (Figure S13, SI), the absorption efficiencies at 362 nm follow the order TNP (H_2O) > TNP (DMF) > 4-NP > 3-NP >*o*-NT >*m*-NT ≈ NB ≈ NM. Furthermore, the hydroxyl groups can interact with the free Lewis-base sites (pyridine rings in **2a**) of the fluorophore through electrostatic interactions and consequently result in a higher quenching effect.[20c,23] The order of the quenching efficiency in DMF was found to be TNP > 4-NP > 3-NP, which is in agreement with the order of acidity of these analytes. This result establishes that electron transfer, energy absorption by the analytes, and electrostatic interaction are synergetic in enhancing the quenching efficiency for TNP in DMF. Due to the strong acidity of TNP in water, the hydroxyl group dissociates easily to form the free anion, which is not likely to accept electrons. The higher quenching constant for TNP in aqueous system is attributed to the higher energy absorption efficiency and the protonated effect of the pyridine rings in the fluorophore.

The remarkable sensing performance of **2a** in suspension motivated us to investigate its sensing capabilities in the detection of TNP in vapor phase.[2d,6c,22c,24] The PL spectra of **2a** deposited on a quartz slide was monitored, before and after exposing it to the equilibrated vapor of TNP at a specified exposure time (0.5, 1, 2.5, 5, 7.5, 10, 15, and 20 min; Figure S14, SI). Rapid response to the TNP vapor was observed; within 0.5 min, a quenching percentage of nearly 20% was reached. At longer exposure time, the quenching percentage almost reached a constant of about 25%. The host skeleton of **2a** is the first example of a MOF-based luminescent sensor for TNP in a pure aqueous

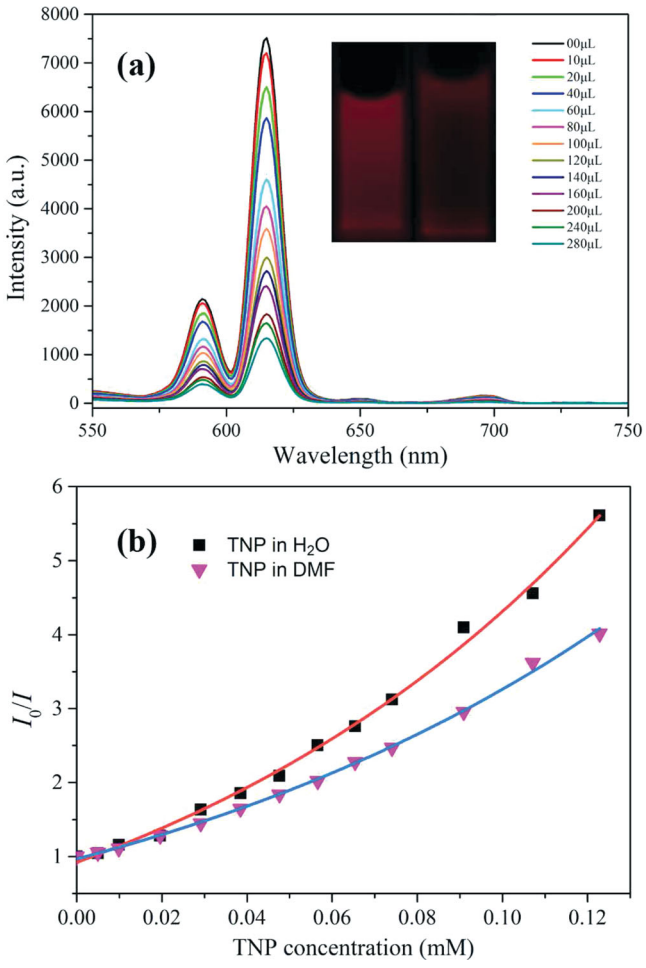

Figure 5. a) Effect on the emission spectra of **2a** dispersed in H_2O upon incremental addition of a TNP aqueous solution (1 mM) (λ_{ex} = 362 nm). Legend indicates the overall concentration of TNP.Inset: A photograph showing the original fluorescence (left) and the quenching fluorescence (right) upon addition of 280 μL TNP (UV light, 365 nm). b) Stern–Volmer plots of I_0/I versus the TNP concentration in DMF and water.

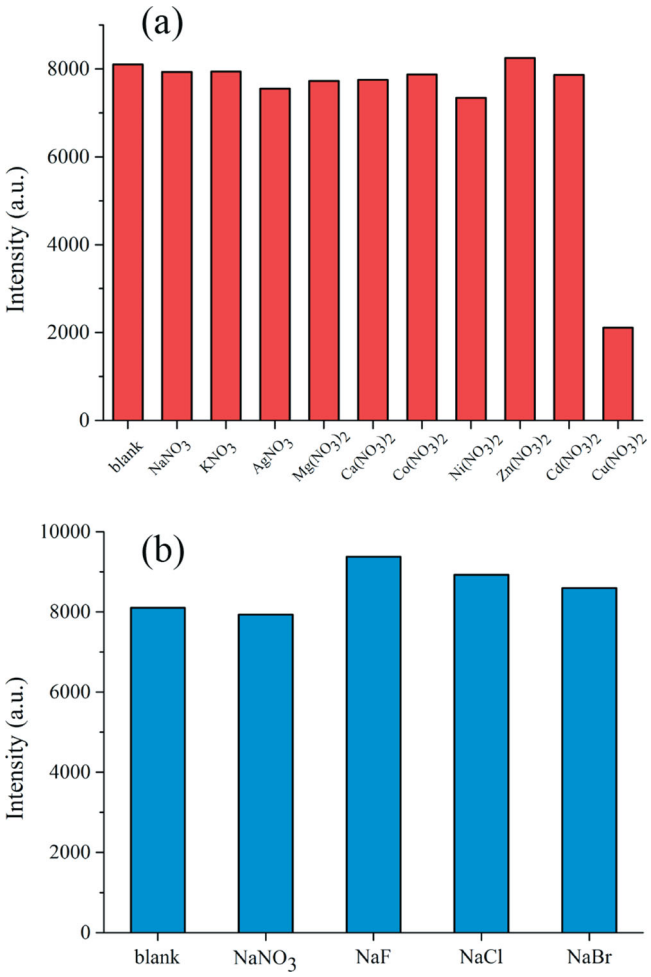

Figure 6. The $^5D_0 \rightarrow {}^7F_2$ transition intensities of ion–**2a** solid samples (λ_{ex} = 362 nm): a) metal ions; b) inorganic anions.

system and in the vapor state; this indicates significant potential for applications in the detection of underwater explosives and environmental monitoring near artillery bases.

2.6. Detection of Metal Cations and Inorganic Anions

The hydrothermal stability of **2a** further prompted us to investigate its ability to sense metal cations and inorganic anions because they can be crucial components in water and are often pollutants. Activated **2a** was immersed in 0.01 mol/L aqueous solutions of various $M(NO_3)_x$ compounds, where M is a variety of metals; it was then filtered, washed, and dried to obtain metal-ion-incorporated M^{x+}–**2a** solid samples. Interestingly, the luminescent intensities of the metal-ion-incorporated M^{x+}–**2a** samples are strongly dependent on the metal ions. The Cu^{2+} ion has the most significant quenching effect on the luminescent intensity, whereas other metal ions show negligible effect on the luminescent intensity (**Figure 6**a). The N 1s X-ray photoelectron spectroscopy (XPS) peak from free pyridyl nitrogen atoms at 398.5 eV in **2a** is shifted to 399.0 eV in Cu^{2+}–**2a**, indicating the weak binding of the pyridyl nitrogen atoms to the Cu^{2+} ion.[25] The bonding interaction is expected to perturb the electronic structure of the ligand and minimize the energy-transfer efficiency from the ligand to the Eu^{3+} centers, thus decreasing the luminescent intensity. The quenching effect of Cu^{2+} is further confirmed by a reduction in fluorescence lifetime of $^5D_0$ from 257.6 μs in **2a** to 193.7 μs in Cu^{2+}–**2a**.

The same procedure was carried out to investigate the sensing function with respect to anions, using NaX (where X = NO_3^-, F^-, Cl^-, and Br^-) aqueous solutions. The luminescent intensity of F^--incorporated **2a** is larger than other anion-incorporated samples (Figure 6b). It was postulated that F^- anions are more easily immobilized within the micropores forming hydrogen bonding interactions with the terminal-ligand water molecules. These interactions reduce the bond stretching of OH oscillators, and therefore enhance the luminescent intensity.[26] In summary, the easily accessible Lewis-base sites and the terminal water molecules in **2a** make it potentially useful for analyzing ionic pollutants in waste water.

3. Conclusion

In summary, a hydrothermally robust, luminescent microporous EuMOF-based sensor was obtained by a SC–SC transformation. Different signal transmission media were introduced into the luminescent host material by pre- and post-synthetic methods. The host material may serve as a multi-responsive luminescent sensor, capable of detecting the organic molecule acetone, discriminating between the homologues and isomers of aliphatic alcohols, as well as sensing highly explosive TNP and inorganic ions in water. This work demonstrates that luminescent MOFs may be rationally designed to serve as practical multi-responsive sensors for the detection of pollutants.

4. Experimental Section

Synthesis of **1**: A mixture of $Eu(NO_3)_3{\cdot}6H_2O$ (0.0225 g, 0.05 mmol), $bpydbH_2$ (0.0198 g, 0.05 mmol), terephthalic acid (0.0082 g, 0.05 mmol), DMF (6.0 mL), and H_2O (1.0 mL) was added to a 15-mL Teflon-lined stainless-steel autoclave and heated at 160 °C for 72 h. After it was cooled to room temperature over a period of 27 h, light yellow, rectangular-prismatic crystals were obtained (52% yield based on $bpydbH_2$). Elemental analysis (Elem. anal.): Calculated (Calcd) for $C_{85}H_{77}Eu_3N_{10}O_{22}$: C, 49.89%; H, 3.79%; N, 6.84%. Found: C, 50.02%; H, 3.74%; N, 6.81%.

Synthesis of **2**: Air-dried crystals of **1** were immersed in MeOH for 4 days, and sequentially in acetone for 2 days. During this period, the MeOH or acetone solvent was periodically refreshed with pure solvent. After decanting the solvent, air-dried crystals of **2**, which were suitable for X-ray diffraction analysis, were obtained (94% yield). Elem. anal.: Found: C, 49.56%; H, 3.23%; N, 4.54%.

Preparation of **2a**: A sample of **2** was activated under vacuum at 150 °C for 15 h, giving rise to activated **2a**. Elem. anal.: Found: C, 50.44%; H, 2.76%; N, 4.83%.

Crystal Data:**1**) $C_{85}H_{77}N_{10}O_{22}Eu_3$; refined formula weight, M_r = 2046.45 g mol^{-1}; monoclinic, $P2_1/n$, a = 14.6534(5) Å, b = 17.7687(6) Å, c = 31.9462(10) Å, β = 90.2920(10)°, V = 8317.8(5) $Å^3$; Z = 4; calculated cell density, D_c = 1.634 g cm^{-3}; reflections collected/independent: 45880/16516; R_{int} = 0.0379; final R_1 = 0.0374 ($I > \sigma(I)$), wR_2 = 0.0993 (all data), GOF = 1.083. **2**) $C_{73}H_{47}N_6O_{17}Eu_3$, M_r = 1736.05; monoclinic, $P2_1/n$, a = 14.5551(5) Å, b = 17.8237(7) Å, c = 31.7548(11) Å, β = 90.9390(10)°, V = 8236.9(5) $Å^3$; Z = 4; D_c = 1.400 g cm^{-3}; reflections collected/independent: 45516/16328; R_{int} = 0.0526. After using the SQUEEZE command, the final R_1 = 0.0425 ($I > \sigma(I)$), wR_2 = 0.1131 (all data), GOF =

0.983. Supplementary crystallographic data for this paper can be obtained free of charge from The Cambridge Crystallographic Data Centre (CCDC) via www.ccdc.cam.ac.uk/data_request/cif: CCDC 966494 (**1**) and 966495 (**2**).

Supporting Information

Supporting Information is available from the Wiley Online Library or from the author.

Acknowledgements

The authors are grateful to the financial aid from the National Natural Science Foundation of China (Grant Nos. 21371165, 51372242, 91122030 and 21210001), and National Natural Science Foundation for Creative Research Group (Grant No. 21221061).

Received: November 26, 2013
Revised: January 16, 2014
Published online: March 18, 2014

[1] a) S. Kitagawa, R. Kitaura, S. Noro, *Angew. Chem.* **2004**, *116*, 2388; *Angew. Chem. Int. Ed.* **2004**, *43*, 2334; b) A. Dhakshinamoorthy, H. Garcia, *Chem. Soc. Rev.* **2012**, *41*, 5262; c) M. Yoon, R. Srirambalaji, K. Kim, *Chem. Rev.* **2012**, *112*, 1196; d) J.-R. Li, J. Sculley, H.-C. Zhou, *Chem. Rev.* **2012**, *112*, 869; e) J.-S. Qin, D.-Y. Du, W.-L. Li, J.-P. Zhang, S.-L. Li, Z.-M. Su, X.-L. Wang, Q. Xu, K.-Z. Shao, Y.-Q. Lan, *Chem. Sci.* **2012**, *3*, 2114.

[2] a) Y. Takashima, V. M. Martínez, S. Furukawa, M. Kondo, S. Shimomura, H. Uehara, M. Nakahama, K. Sugimoto, S. Kitagawa, *Nat. Commun.* **2011**, *2*, 168; b) Y.-Q. Chen, G.-R. Li, Z. Chang, Y.-K. Qu, Y.-H. Zhang, X.-H. Bu, *Chem. Sci.* **2013**, *4*, 3678; c) Z.-Z. Lu, R. Zhang, Y.-Z. Li, Z.-J. Guo, H.-G. Zheng, *J. Am. Chem. Soc.* **2011**, *133*, 4172; d) A. Lan, K. Li, H. Wu, D. H. Olson, T. J. Emge, W. Ki, M. Hong, J. Li, *Angew. Chem.* **2009**, *121*, 2370; *Angew. Chem. Int. Ed.* **2009**, *48*, 2334; e) J. Ferrando-Soria, P. Serra-Crespo, M. de Lange, J. Gascon, F. Kapteijn, M. Julve, J. Cano, F. Lloret, J. Pasán, C. Ruiz-Pérez, Y. Journaux, E. Pardo, *J. Am. Chem. Soc.* **2012**, *134*, 15301; f) J. Ferrando-Soria, H. Khajavi, P. Serra-Crespo, J. Gascon, F. Kapteijn, M. Julve, F. Lloret, J. Pasán, C. Ruiz-Pérez, Y. Journaux, E. Pardo, *Adv. Mater.* **2012**, *24*, 5625; g) G. Lu, J. T. Hupp, *J. Am. Chem. Soc.* **2010**, *132*, 7832.

[3] a) B. V. Harbuzaru, A. Corma, F. Rey, J. L. Jorda, D. Ananias, L. D. Carlos, J. Rocha, *Angew. Chem.* **2009**, *121*, 6958; *Angew. Chem. Int. Ed.* **2009**, *48*, 6476; b) X. Rao, T. Song, J. Gao, Y. Cui, Y. Yang, C. Wu, B. Chen, G. Qian, *J. Am. Chem. Soc.* **2013**, *135*, 15559; c) S. Dang, E. Ma, Z.-M. Sun, H. Zhang, *J. Mater. Chem.* **2012**, *22*, 16920; d) H. Xu, X. Rao, J. Gao, J. Yu, Z. Wang, Z. Dou, Y. Cui, Y. Yang, B. Chen, G. Qian, *Chem. Commun.* **2012**, *48*, 7377; e) Y. Li, S. Zhang, D. Song, *Angew. Chem.* **2013**, *125*, 738; *Angew. Chem. Int. Ed.* **2013**, *52*, 710; f) K.-L. Wong, G.-L. Law, Y.-Y. Yang, W.-T. Wong, *Adv. Mater.* **2006**, *18*, 1051; g) P. Wu, J. Wang, Y. Li, C. He, Z. Xie, C. Duan, *Adv. Funct. Mater.* **2011**, *21*, 2788.

[4] a) J. M. Falkowski, C. Wang, S. Liu, W. Lin, *Angew. Chem.* **2011**, *123*, 8833; *Angew. Chem. Int. Ed.* **2011**, *50*, 8674; b) K. S. Jeong, Y. B. Go, S. M. Shin, S. J. Lee, J. Kim, O. M. Yaghi, N. Jeong, *Chem. Sci.* **2011**, *2*, 877; c) A. M. Shultz, O. K. Farha, D. Adhikari, A. A. Sarjeant, J. T. Hupp, S. T. Nguyen, *Inorg. Chem.* **2011**, *50*, 3174; d) M.-H. Xie, X.-L. Yang, C. Zou, C.-D. Wu, *Inorg. Chem.* **2011**, *50*, 5318; e) F. Song, C. Wang, J. M. Falkowski, L. Ma, W. Lin, *J. Am. Chem. Soc.* **2010**, *132*, 15390; f) C. Wang, Z. Xie, K. E. deKrafft, W. Lin, *J. Am. Chem. Soc.* **2011**, *133*, 13445.

[5] a) H. J. Park, M. P. Suh, *Chem. Sci.* **2013**, *4*, 685; b) T. K. Prasad, D. H. Hong, M. P. Suh, *Chem. Eur. J.* **2010**, *16*, 14043; c) S. M. Cohen, *Chem. Rev.* **2012**, *112*, 970; d) X.-J. Wang, P.-Z. Li, L. Liu, Q. Zhang, P. Borah, J. D. Wong, X. X. Chan, G. Rakesh, Y. Lia, Y. Zhao, *Chem. Commun.* **2012**, *48*, 10286; e) C. K. Brozek, M. Dincă, *J. Am. Chem. Soc.* **2013**, *135*, 12886.

[6] a) S. Mohapatra, B. Rajeswaran, A. Chakraborty, A. Sundaresan, T. K. Maji, *Chem. Mater.* **2013**, *25*, 1673; b) Q. Tang, S. Liu, Y. Liu, J. Miao, S. Li, L. Zhang, Z. Shi, Z. Zheng, *Inorg. Chem.* **2013**, *52*, 2799; c) A. K. Chaudhari, S. S. Nagarkar, B. Joarder, S. K. Ghosh, *Cryst. Growth Des.* **2013**, *13*, 3716; d) G.-Y. Wang, L.-L. Yang, Y. Li, H. Song, W.-J. Ruan, Z. Chang, X.-H. Bu, *Dalton Trans.* **2013**, *42*, 12865; e) X. Zhou, H. Li, H. Xiao, L. Li, Q. Zhao, T. Yang, J. Zuo, W. Huang, *Dalton Trans.* **2013**, *42*, 5718; f) Y. Xiao, Y. Cui, Q. Zheng, S. Xiang, G. Qian, B. Chen, *Chem. Commun.* **2010**, *46*, 5503.

[7] a) L. Hou, W.-X. Zhang, J.-P. Zhang, W. Xue, Y.-B. Zhang, X.-M. Chen, *Chem. Commun.* **2010**, *46*, 6311; b) J. Park, J.-R. Li, E. C. Sañudo, D. Yuan, H.-C. Zhou, *Chem. Commun.* **2012**, *48*, 883; c) M. K. Sharma, I. Senkovska, S. Kaskel, P. K. Bharadwaj, *Inorg. Chem.* **2011**, *50*, 539; d) S.-Y. Song, X.-Z. Song, S.-N. Zhao, C. Qin, S.-Q. Su, M. Zhu, Z.-M. Hao, H.-J. Zhang, *Dalton Trans.* **2012**, *41*, 10412; e) Y.-S. Wei, K.-J. Chen, P.-Q. Liao, B.-Y. Zhu, R.-B. Lin, H.-L. Zhou, B.-Y. Wang, W. Xue, J.-P. Zhang, X.-M. Chen, *Chem. Sci.* **2013**, *4*, 1539.

[8] a) A. D. Burrows, K. Cassar, T. Duren, R. M. Friend, M. F. Mahon, S. P. Rigby, T. L. Savarese, *Dalton Trans.* **2008**, 2465; b) Z.-J. Lin, Z. Yang, T.-F. Liu, Y.-B. Huang, R. Cao, *Inorg. Chem.* **2012**, *51*, 1813.

[9] a) R. Feng, L. Chen, Q.-H. Chen, X.-C. Shan, Y.-L. Gai, F.-L. Jiang, M.-C. Hong, *Cryst. Growth Des.* **2011**, *11*, 1705; b) W.-H. Zhu, Z.-M. Wang, S. Gao, *Inorg. Chem.* **2007**, *46*, 1337; c) J. Fan, Z.-H. Wang, M. Yang, X. Yin, W.-G. Zhang, Z.-F. Huang, R.-H. Zeng, *Cryst. Eng. Commun.* **2010**, *12*, 216; d) J.-C. G. Bünzli, F. Ihringer, P. Dumy, C. Sager, R. D. Rogers, *J. Chem. Soc., Dalton Trans.* **1998**, 497.

[10] a) N. L. Rosi, J. Kim, M. Eddaoudi, B. Chen, M. O'Keeffe, O. M. Yaghi, *J. Am. Chem. Soc.* **2005**, *127*, 1504; b) Y. He, S. Xiang, Z. Zhang, S. Xiong, F. R. Fronczek, R. Krishna, M. O'Keeffe, B. Chen, *Chem. Commun.* **2012**, *48*, 10856.

[11] A. L. Spek, *J. Appl. Crystallogr.* **2003**, *36*, 7.

[12] a) S. Viswanathan, A. de Bettencourt-Dias, *Inorg. Chem.* **2006**, *45*, 10138; b) D. C. Wilson, S. Liu, X. Chen, E. A. Meyers, X. Bao, A. V. Prosvirin, K. R. Dunbar, C. M. Hadad, S. G. Shore, *Inorg. Chem.* **2009**, *48*, 5725; c) Y. Li, D. Song, *Cryst. Eng. Commun.* **2011**, *13*, 1821.

[13] a) K. S. Park, Z. Ni, A. P. Cote, J. Y. Choi, R. Huang, F. J. Uribe-Romo, H. K. Chae, M. O'Keeffe, O. M. Yaghi, *Proc. Natl. Acad. Sci. U. S. A.* **2006**, *103*, 10186; b) H. J. Choi, M. Dincă, A. Dailly, J. R. Long, *Energy Environ. Sci.* **2010**, *3*, 117; c) V. Colombo, S. Galli, H. J. Choi, G. D. Han, A. Maspero, G. Palmisano, N. Masciocchi, J. R. Long, *Chem. Sci.* **2011**, *2*, 1311; d) J. Duan, M. Higuchi, S. Horike, M. L. Foo, K. P. Rao, Y. Inubushi, T. Fukushima, S. Kitagawa, *Adv. Funct. Mater.* **2013**, *23*, 3525.

[14] a) J. J. Low, A. I. Benin, P. Jakubczak, J. F. Abrahamian, S. A. Faheem, R. R. Willis, *J. Am. Chem. Soc.* **2009**, *131*, 15834; b) I. J. Kang, N. A. Khan, E. Haque, S. H. Jhung, *Chem. Eur. J.* **2011**, *17*, 6437.

[15] a) Y. Xiao, L. Wang, Y. Cui, B. Chen, F. Zapata, G. Qian, *J. Alloy. Compd.* **2009**, *484*, 601; b) W. Yang, J. Feng, S. Song, H. Zhang, *ChemPhysChem* **2012**, *13*, 2734; c) Z. Hao, X. Song, M. Zhu, X. Meng, S. Zhao, S. Su, W. Yang, S. Song, H. Zhang, *J. Mater. Chem. A* **2013**, *1*, 11043.

[16] B. Chen, Y. Yang, F. Zapata, G. Lin, G. Qian, E. B. Lobkovsky, *Adv. Mater.* **2007**, *19*, 1693.

[17] a) F.-Y. Yi, W. Yang, Z.-M. Sun, *J. Mater. Chem.* **2012**, *22*, 23201; b) H. Li, W. Shi, K. Zhao, Z. Niu, H. Li, P. Cheng, *Chem. Eur. J.* **2013**, *19*, 3358.

[18] a) J. Liu, Y. Zhong, P. Lu, Y. Hong, J. W. Y. Lam, M. Faisal, Y. Yu, K. S. Wong, B. Z. Tang, *Polym. Chem.* **2010**, *1*, 426; b) X.-H. Zhou, L. Li, H.-H. Li, A. Li, T. Yang, W. Huang, *Dalton Trans.* **2013**, *42*, 12403.

[19] B. Gole, S. Shanmugaraju, A. K. Bar, P. S. Mukherjee, *Chem. Commun.* **2011**, *47*, 10046.

[20] a) A. Saxena, M. Fujiki, R. Rai, G. Kwak, *Chem. Mater.* **2005**, *17*, 2181; b) J. C. Sanchez, A. G. DiPasquale, A. L. Rheingold, W. C. Trogler, *Chem. Mater.* **2007**, *19*, 6459; c) S. S. Nagarkar, B. Joarder, A. K. Chaudhari, S. Mukherjee, S. K. Ghosh, *Angew. Chem.* **2013**, *125*, 2953; *Angew. Chem. Int. Ed.* **2013**, *52*, 2881.

[21] D. Li, J. Liu, R. T. K. Kwok, Z. Liang, B. Z. Tang, J. Yu, *Chem. Commun.* **2012**, *48*, 7167.

[22] a) H. Sohn, M. J. Sailor, D. Magde, W. C. Trogler, *J. Am. Chem. Soc.* **2003**, *125*, 3821; b) S. J. Toal, J. C. Sanchez, R. E. Dugan, W. C. Trogler, *J. Forensic Sci.* **2007**, *52*, 79; c) S. Pramanik, C. Zheng, X. Zhang, T. J. Emge, J. Li, *J. Am. Chem. Soc.* **2011**, *133*, 4153.

[23] a) G. He, H. Peng, T. Liu, M. Yang, Y. Zhang, Y. Fang, *J. Mater. Chem.* **2009**, *19*, 7347; b) Y. Peng, A.-J. Zhang, M. Dong, Y.-W. Wang, *Chem. Commun.* **2011**, *47*, 4505.

[24] Z. Hu, S. Pramanik, K. Tan, C. Zheng, W. Liu, X. Zhang, Y. J. Chabal, J. Li, *Cryst. Growth Des.* **2013**, *13*, 4204.

[25] B. Chen, L. Wang, Y. Xiao, F. R. Fronczek, M. Xue, Y. Cui, G. Qian, *Angew. Chem.* **2009**, *121*, 508; *Angew. Chem. Int. Ed.* **2009**, *48*, 500.

[26] B. Chen, L. Wang, F. Zapata, G. Qian, E. B. Lobkovsky, *J. Am. Chem. Soc.* **2008**, *130*, 6718.